J Mar Sci Technol (2011) 16:472–490
DOI 10.1007/s00773-011-0140-3

ORIGINAL ARTICLE

Manoeuvring characteristics of twin-rudder systems: rudder-hull interaction effect on the manoeuvrability of twin-rudder ships

Sahbi Khanfir · Kazuhiko Hasegawa · Vishwanath Nagarajan · Kouichi Shouji · Seung Keon Lee

Received: 10 November 2010 / Accepted: 7 August 2011 / Published online: 21 September 2011

Abstract With a recent increase in ship capacity and propulsion performance, a wide-beam ship fitted with a twin-rudder system has been adopted in many cases. However, to improve ship manoeuvring, it is still necessary to have a better understanding of rudder-hull interactions in twin-rudder ships. Captive model tests (oblique towing and circular motion test) as well as free-running tests with a single-propeller twin-rudder ship and a twin-propeller twin-rudder ship are carried out. The effect of drift angle on the rudder forces and some peculiar phenomena concerning rudder normal force for twin-rudder ships are evaluated. A method for estimating the hull-rudder interaction coefficients based on free-running experimental results is proposed.

Keywords Single-propeller twin-rudder system · Twin-propeller twin-rudder system · Rudder normal force · Hull-rudder interaction coefficients

The subscripts in parenthesis 'S' and 'P' refer to starboard and port twin-propeller twin-rudder, respectively. The expression for single-propeller single-rudder is defined by removing the subscript 'S' and 'P' in the parenthesis.

S. Khanfir (✉) · K. Hasegawa
Department of Naval Architecture and Ocean Engineering, Graduate School of Engineering, Osaka University, 2-1 Yamadaoka, Suita 565-0871, Japan
e-mail: khanfir@naoe.eng.osaka-u.ac.jp

V. Nagarajan
Department of Ocean Engineering and Naval Architecture, Indian Institute of Technology Kharagpur, Kharagpur 721 302, West Bengal, India

K. Shouji
IHI Corporation, 1, Shin-Nakahara-cho, Isogo-ku, Yokohama 235-8501, Japan

S. K. Lee
Department of Naval Architecture and Ocean Engineering, Pusan National University, Gumjeong-gu, Busan 609-735, Korea

List of symbols

a_H	Interaction force coefficient induced on ship hull by rudder normal force
B	Ship's breadth (m)
C_B	Block coefficient
C_R	Rudder chord (m)
d	Ship's mean draft (m)
$D_{P(S)}$ (P)	Diameter of starboard and port propeller (m)
$F_{RY(S)}$ (P)	Normal force for starboard and port rudder (N)
$F_{RX(S)}$ (P)	Axial force for starboard and port rudder (N)
H_R	Rudder height for starboard and port rudder (m)
I_{zz}	Yaw moment of inertia (kg/m^2)
$J_{P(S)}$ (P)	Real advance ratio for starboard and port propeller
$J_{S(S)}$ (P)	Apparent advance ratio for starboard and port propeller
J_{zz}	Added yaw moment of inertia (kg/m^2)
$K_{T(S)}$ (P)	Thrust coefficient for starboard and port propeller
L	Ship's length (m)
LCG	Ship's longitudinal centre of gravity (m)
$L_{R(S)}$ (P)	Flow-straightening coefficient of yaw rate for starboard and port rudder (m)
m	Ship's mass (kg)
m_x	Added mass in surge (kg)
m_y	Added mass in sway (kg)

$n_{(S)(P)}$ Starboard and port propeller revolution (rps)
N_H Hydrodynamic yaw moment due to ship's sway and yaw motions acting at ship's LCG (Nm)
N_R Hydrodynamic yaw moment due to rudder acting at ship's LCG (Nm)
$P_{(S)(P)}$ Main propeller pitch of starboard and port propeller (m)
r Yaw rate of ship (rad/s)
$\dot{r}$ Yaw acceleration of ship (rad/s^2)
$S_{(S)(P)}$ Propeller slip ratio of starboard and port propeller
$S_{R(S)(P)}$ Area of starboard and port rudder (m^2)
S_W Ship's wetted surface area excluding rudder's wetted surface area (m^2)
$t_{P(S)(P)}$ Thrust deduction factor in manoeuvring for starboard and port propeller
$t_{R(S)(P)}$ Coefficient for reduction of rudder's resistance in ship's surge direction for starboard and port rudder
u Ship's surge velocity (m/s)
$u_{P(S)(P)}$ Effective inflow velocity to starboard and port propeller (m/s)
$u_{R(S)(P)}$ Inflow velocity in surge direction to starboard and port rudder (m/s)
$\dot{u}$ Ship's surge acceleration (m/s^2)
$U = \sqrt{u^2 + v^2}$ Ship's velocity (m/s^2)
$U_{R(S)(P)}$ Inflow velocity to starboard and port rudder (m/s)
v Ship's sway velocity (m/s)
$v_{R(S)(P)}$ Inflow velocity in sway direction to starboard and port rudder (m/s)
$\dot{v}$ Ship's sway acceleration (m/s^2)
$w_{P0(S)(P)}$ Effective propeller wake fraction in straight running for starboard and port propeller
$w_{P(S)(P)}$ Effective propeller wake fraction in manoeuvring for starboard and port propeller
$w_{R(S)(P)}$ Effective wake fraction for starboard and port rudder
x_G Location of ship's centre of gravity in X-axis (m)
x_H Location of acting point of interaction force induced on ship hull by rudder normal force (m)
$x_{P(S)(P)}$ Location of propeller in X-axis for starboard and port propeller (m)
$x_{R(S)(P)}$ Location of rudder in X-axis for starboard and port rudder (m)
X_H Hydrodynamic surge force due to ship's sway and yaw motions acting on ship's LCG (N)
X_P Hydrodynamic surge force due to propeller acting on ship's LCG (N)
X_R Hydrodynamic surge force due to rudder acting on ship's LCG (N)
Y_H Hydrodynamic sway force due to ship's sway and yaw motions acting on ship's LCG (N)
$y_{P(S)(P)}$ Location of propeller in Y-axis for starboard and port propeller (m)
$y_{R(S)(P)}$ Location of rudder in Y-axis for starboard and port rudder (m)
Y_P Hydrodynamic sway force due to rudder acting on ship's LCG (N)
Y_R Hydrodynamic sway force due to rudder acting on ship's LCG (N)
$\alpha_{(S)(P)}$ Axial distance between rudder and propeller (m)
$\alpha_{R(S)(P)}$ Effective inflow angle to starboard and port rudder (rad)
β Drift angle of ship (rad)
$\beta_{R(S)(P)}$ Effective drift angle at rudder position for starboard and port rudder (rad)
$\gamma_{R(S)(P)}$ Flow-straightening coefficient of sway velocity for starboard and port rudder
$\delta_{R(S)(P)}$ Angle of starboard and port rudder (rad)
$\delta_{0(S)(P)}$ Hydrodynamic neutral angle for starboard and port rudder (rad)
$\delta_{(S)(P)(P)(S)}$ Variation of inflow rudder angle due to interaction between starboard and port rudder (rad)
$\delta_{R(S)(P)}$ Effective rudder angle at which the rudder normal force becomes zero for starboard and port rudder (rad)
$\varepsilon_{(S)(P)}$ Ratio of effective wake fraction in way of propeller and rudder for starboard and port rudder
$\kappa_{(S)(P)}$ Propeller race amplification factor for starboard and port rudder
ρ Water density (kg/m^3)
ψ Ship's heading angle (rad)

1 Introduction

Recently, there is demand for increasing ship-size and speed, while simultaneously maintaining good manoeuvrability and minimum draft of the ship. Different

combinations of the multi-propeller multi-rudder system are being investigated for the new design of ships. There is a well-established MMG model that has been developed in Japan since 1970s [1] for manoeuvring studies of single-propeller single-rudder ships. For the MMG model, some database or estimation charts are available to estimate the coefficients of the mathematical model for various types of ships. The MMG model has also been expanded for shallow water and a twin-propeller twin-rudder system. This is because for shallow water, a twin-propeller twin-rudder system is usually preferred due to restrictions in draft and the requirement for increased manoeuvrability. However, for a twin-propeller twin-rudder system, only limited data are available, and it is sufficient to estimate the coefficients for any given unknown ship. Twin-propeller twin-rudder ships for merchant ship application are usually wider than single-propeller single-rudder ships. Therefore, their manoeuvring characteristics are remarkably different. Consequently, it is important to study the different manoeuvring characteristics of wide-beam ships fitted with a twin-propeller twin-rudder system. A better understanding of its hull-rudder interactions is important to improve the accuracy of the mathematical manoeuvring models intended for a wide range of usage from harbour to cruising speed manoeuvres. Theoretical and experimental researches have been carried out to investigate the manoeuvring ability of a twin-propeller twin-rudder system from various viewpoints. Lee et al. [2, 3] extended the applicability of the MMG model to twin-propeller twin-rudder ships. They modified the mathematical model of the propeller wake for a twin-propeller twin-rudder ship based on CMT experiment data. Yoshimura and Sakurai [4] studied the manoeuvring characteristics of conventional and wide-beam twin-propeller twin-rudder ships at different water depths. The mechanism of shallow water effects on rudder and hull force was investigated. It was shown that some twin-propeller twin-rudder ships could differ significantly in their turning and course keeping qualities when compared with conventional ships in shallow water. The study concluded that an MMG-type mathematical model is also suitable for a twin-propeller twin-rudder ship and a model with all the hydrodynamic coefficients for deep and shallow water was provided. Nakatake et al. [5] investigated the interaction between the ship hull, propellers, and rudders. They concluded that the propulsive efficiency of the propeller-rudder system significantly depends on rudder drag. Fung et al. [6] investigated the influence of the ship's aftbody, especially the stern form, on the interaction forces and the steering effect of the twin-propeller in different modes of operations. Among the three typical aftbody shapes (conventional, twin-skeg, and twin-tail) the twin-skeg ship provided the best manoeuvrability.

Similarly, single-propeller twin-rudder systems are also being investigated for large vessels. The single-propeller twin-rudder system has been successfully installed on coastal ships because of their good manoeuvring performance. Regarding coastal ships, narrow channels' and harbours' manoeuvring hours are quite significant. Theoretical and experimental studies have investigated the manoeuvring ability of a single-propeller twin-rudder system from various viewpoints. The MMG-type model for a single-propeller twin-rudder ship has been developed [7]. Accordingly, the suitability of a single-propeller twin-rudder system for large ships from the aspect of manoeuvring has been confirmed [8] and its variant for large ships has been proposed [9]. An MMG-type manoeuvring model for a single-propeller twin-rudder system for large ships has been developed [10] and its suitability for large ships from the aspect of manoeuvring and propulsion has been confirmed [11]. From the above studies, it is concluded that for the same maximum ship dimensions, the single-propeller twin-rudder system due to its compact size and high lift force could improve a ship's cargo carrying capacity and its manoeuvring ability when compared to the single-propeller single-rudder system.

This work is a further extension of our investigation on the twin-rudder system with either a single or twin-propeller [12]. In this study, the following aspects are investigated:

(a) The hull rudder interaction coefficients for a single-propeller twin-rudder ship and twin-propeller twin-rudder ship; and
(b) A method to estimate the flow-straightening coefficient from free-running experiment data.

2 Mathematical model for a multi-propeller multi-rudder ship

The MMG-type modular manoeuvring model [1] for a multi-propeller multi-rudder ship will be described. For

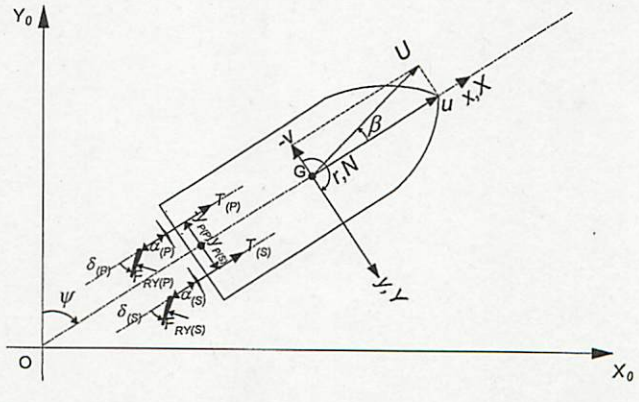

Fig. 1 Coordinate system for twin-rudder ships

this study, single-propeller single-rudder, single-propeller twin-rudder, and twin-propeller twin-rudder ships will be hereafter referred to as SPSR, SPTR, and TPTR ships.

2.1 Coordinate system, equations of motion and mathematical model

A three degree-of-freedom (surge, sway, and yaw) model is considered for the ship's manoeuvring motions. The coordinate system for the TPTR system is shown in Fig. 1. Regarding the SPTR system, there will be one single propeller located on the ship's centreline, while for the SPSR system, both propeller and rudder are positioned along the ship's centreline. The equations of surge, sway, and yaw motion considering the origin of the coordinate system located at the ship's centre of gravity is expressed as shown in Eq. 1.

$$\begin{aligned}(m+m_x)\dot{u}-(m+m_y)vr &= X_H+X_P+X_R\\ (m+m_y)\dot{v}+(m+m_x)ur &= Y_H+Y_P+Y_R\\ (I_{zz}+J_{zz})\dot{r} &= N_H+N_P+N_R\end{aligned} \tag{1}$$

The subscripts 'H', 'P,' and 'R' refer to hull, propeller, and rudder, respectively. For the SPTR system, the hydrodynamic forces and moment acting on the hull were determined as per Kijima's [13] regression formula. For the TPTR system, the hydrodynamic forces and moment acting on the hull are expressed as shown in Eq. 2.

$$\left.\begin{aligned}X_H &= \frac{1}{2}\rho L d U^2(X'_0+X'_{|v|}|v'|+X'_{|r|}|r'|+X'_{vv}(v')^2\\ &\quad +X'_{vr}v'r'+X'_{rr}(r')^2)\\ Y_H &= \frac{1}{2}\rho L d U^2(Y'_v v'+Y'_r r'+Y'_{vvv}(v')^3\\ &\quad +Y'_{vvr}(v')^2 r'+Y'_{vrr}v'(r')^2+Y'_{rrr}(r')^3)\\ N_H &= \frac{1}{2}\rho L^2 d U^2(N'_v v'+N'_r r'+N'_{vvv}(v')^3\\ &\quad +N'_{vvr}(v')^2 r'+N'_{vrr}v'(r')^2+N'_{rrr}(r')^3)\end{aligned}\right\} \tag{2}$$

The ships used for this study are a panamax tanker (model ship A) and a shallow-draft heavy-cargo carrier (model ship B). These types of ships are usually fitted with fixed pitch propellers (FPP). Therefore, FPP propellers were used and modelled in the present study. The sway and yaw terms due to propeller (Y_P and N_P) are considered only for the TPTR ship, since each propeller is physically offset from the ship's centreline. For the SPSR and SPTR model ships, the propeller is rotating clockwise, while for the TPTR model ship, each one of the propellers is turning outward over the top. Since each propeller of the TPTR system is an FPP-type that rotates in the opposite direction, the resultant propeller sway force is, therefore, negligible ($Y_P = 0$). In this paper, regarding the propeller and rudder mathematical model, only the expression for the TPTR system will be shown. The expression for the TPTR is shown in Eq. 3, and it can be simplified for the SPTR and SPSR systems.

$$\left.\begin{aligned}X_P &= \rho\{(1-t_{P(S)})n^2_{(S)}D^4_{P(S)}K_{T(S)}(J_{P(S)})\\ &\quad +(1-t_{P(P)})n^2_{(P)}D^4_{P(P)}K_{T(P)}(J_{P(P)})\}\\ N_P &= \rho\{(1-t_{P(S)})y_{P(S)}n^2_{(S)}D^4_{P(S)}K_{T(S)}(J_{P(S)})\\ &\quad +(1-t_{P(P)})y_{P(P)}n^2_{(P)}D^4_{P(P)}K_{T(P)}(J_{P(P)})\}\end{aligned}\right\} \tag{3}$$

The expression for the SPTR and SPSR model ships can be obtained from Eq. 3 by removing the subscript 'S' and 'P' in the parenthesis and by considering $y_{P(S)}=0$. The forces and moment due to the rudder are expressed using Lee et al.'s [2, 3] model as shown in Eq. 4.

$$\left.\begin{aligned}X_R &= -(1-t_{R(S)})F_{RY(S)}\sin\delta_{(S)}\\ &\quad -(1-t_{R(P)})F_{RY(P)}\sin\delta_{(P)})\\ Y_R &= -(1+a_H)(F_{RY(S)}\cos\delta_{(S)}+F_{RY(P)}\cos\delta_{(P)})\\ N_R &= -(x_R+a_H x_H)(F_{RY(S)}\cos\delta_{(S)}\\ &\quad +F_{RY(P)}\cos\delta_{(P)})+f(x_R)\\ f(x_R) &= y_{R(S)}(1-t_{R(S)})F_{RY(S)}\sin\delta_{(S)}\\ &\quad +y_{R(P)}(1-t_{R(P)})F_{RY(P)}\sin\delta_{(P)}\\ t_{R(S)} &= t_{R(P)}\end{aligned}\right\} \tag{4}$$

In the SPSR system, the term $f(x_R)$ in Eq. 4 is omitted, while for SPTR $y_{R(S)}\approx 0$ The rudder normal force is expressed as shown in Eq. 5.

$$F_{RY(S)\,(P)} = \frac{1}{2}\rho S_{R(S)\,(P)}F'_{RY(S)\,(P)}(\alpha_{R(S)\,(P)})U^2_{R(S)\,(P)} \tag{5}$$

In Eq. 5 inside the parenthesis, the top row refers to starboard and the bottom row refers to the port twin-rudder, respectively. This method of writing the equations for both the TPTR and SPTR systems will be followed in the rest of this paper. The effective inflow velocity to the rudder is expressed as shown in Eq. 6.

$$U_{R(S)\,(P)} = \sqrt{u^2_{R(S)\,(P)}+v^2_{R(S)\,(P)}} \tag{6}$$

The effective inflow angle to the rudder for the TPTR system is expressed as shown in Eq. 7.

$$\alpha_{R(S)\,(P)} = \delta_{(S)\,(P)}-\delta_{R(S)\,(P)}(\beta_{R(S)\,(P)}) \tag{7}$$

For the TPTR system, the offset of the rudder from the ship's centreline is included in the effective rudder angle expression as shown in Eq. 8.

$$\delta_{\substack{R(S)\\(P)}} = \gamma_{\substack{R(S)\\(P)}}\beta_{\substack{R(S)\\(P)}} + \tan^{-1}\left(y_{\substack{R(S)\\(P)}}\Big/ x_{\substack{P(S)\\(P)}}\right) \tag{8}$$

The effective inflow angle to the rudder for the SPTR system is expressed as shown in Eq. 9.

$$\alpha_{\substack{R(S)\\(P)}} = \delta_{\substack{(S)\\(P)}} - \delta_{\substack{0(S)\\(P)}} - \delta_{\substack{(S)(P)\\(P)(S)}} - \tan^{-1}\left(v_{\substack{R(S)\\(P)}}\Big/ u_{\substack{R(S)\\(P)}}\right) \tag{9}$$

The effective drift angle at rudder position is defined as shown in Eq. 10.

$$\beta_{\substack{R(S)\\(P)}} = \beta - L_{\substack{R(S)\\(P)}}{}' r' \tag{10}$$

The inflow velocity in the surge direction to the rudder for TPTR and SPTR model ships is expressed as shown in Eq. 11.

$$\left.\begin{aligned} u_{\substack{R(S)\\(P)}} &= \varepsilon_{\substack{(S)\\(P)}} u_{\substack{P(S)\\(P)} } \sqrt{\eta_{\substack{(S)\\(P)}}\left[1+\kappa_{\substack{(S)\\(P)}}\left(\sqrt{1+\frac{8K_{\substack{T(S)\\(P)}}}{\pi J_{\substack{P(S)\\(P)}}{}^2}}-1\right)\right]^2 + \left(1-\eta_{\substack{(S)\\(P)}}\right)} \\ \varepsilon_{\substack{(S)\\(P)}} &= \left(1-w_{\substack{R(S)\\(P)}}\right)\Big/\left(1-w_{\substack{P(S)\\(P)}}\right),\ \kappa_{\substack{(S)\\(P)}} = k_x/\ \varepsilon_{\substack{(S)\\(P)}},\ \eta_{\substack{(S)\\(P)}} = D_{\substack{P(S)\\(P)}}/H_{\substack{R(S)\\(P)}}, \\ u_{\substack{P(S)\\(P)}} &= \left(1-w_{\substack{P(S)\\(P)}}\right)\left(u+y_{\substack{P(S)\\(P)}} r\right) \end{aligned}\right\} \tag{11}$$

For the SPSR system, Eq. 11 can be simplified by removing the subscript 'S' and 'P' in the parenthesis and by taking $y_{\substack{P(S)\\(P)}} = 0$. The inflow velocity in the sway direction to the rudder for TPTR, SPTR, and SPSR models can be expressed as shown in Eqs. 12, 13, and 14.

$$v_{\substack{R(S)\\(P)}} = u_{\substack{R(S)\\(P)}} \tan\left(\delta_{\substack{R(S)\\(P)}}\right) \tag{12}$$

$$v_{\substack{R(S)\\(P)}} = -\gamma_{\substack{R(S)\\(P)}} v - L_{\substack{R(S)\\(P)}} r \tag{13}$$

$$v_R = -\gamma_R (v + L_R r) \tag{14}$$

In Eqs. 12, 13 and 14, the difference in the expression for different rudder systems may be observed.

2.2 Model ships

Two different model ships fitted with different rudder systems were used for this study. The principal particulars of the model ships are shown in Table 1. Model ship A and B are SPTR and TPTR ships, respectively. The model ship A is fitted with a detachable type of stern that can be changed to suit SPSR and TPTR systems, respectively. Three types of rudders, single, twin (type I and type II) were fabricated for the model ship A. A brief description of the twin-rudder system (types I and II) will be given. Each one of the twin-rudders has the Schilling rudder profile, which has a rounded leading edge and a fishtail trailing edge. The twin-rudders are fitted with end plates on the top and bottom part of each rudder. In the twin-rudder (type I), the cross-section of the port and starboard rudder is the same, the rudder cross-section does not have camber, the end plates are flat at the top and knuckled at the bottom and symmetrical about the centreline of each rudder. In the twin-rudder (type II) system, the cross-section of the port and starboard rudder is not symmetrical about its centreline; the rudder cross-section has a cambered profile and the end plates are knuckled and on the outboard side of each rudder. For model ship B, a conventional spade rudder (with NACA cross-section) was fabricated. The layouts of the rudder systems for model ship A and model ship B are shown in Figs. 2 and 3. The particulars of model ship B and other TPTR model ships are shown in Table 2. The lateral distance between rudders and propellers of model ship B is similar to the conventional TPTR system. This distance is higher in the case of wide-beam TPTR ships. The axial distance between rudder and propeller for the subject TPTR system is $\alpha_{\substack{(S)\\(P)}} = 0.77\, D_{\substack{R(S)\\(P)}}$, for the subject SPTR system it is $\alpha_{\substack{(S)\\(P)}} = 0.63\, D_P$ while for conventional ships it is in the range 0.15–0.20 D_P [14].

3 Determination of hull-rudder interaction coefficients for SPSR and SPTR systems

For the SPTR system, it is known that the coefficients $\gamma_{\substack{R(S)\\(P)}}$ and $L_{\substack{R(S)\\(P)}}$ may not be symmetric for the ship's port and

Table 1 Principal particulars of model ships

Particulars	Model ship A	Model ship B
Hull		
L (m)	3.94	4.00
B (m)	0.58	0.85
d (m)	0.22	0.28
LCG/L	0.037	−0.006
C_B	0.83	0.80
S_W (m^2)		
Single-rudder skeg	3.541	N/A
Twin-rudder skeg	3.558	4.9864
Rudder		
H_R (m)	0.1190	0.192
C_R (m)	0.0740	0.139
$S_{R(S)}$ (m^2)[a]	0.0088	0.02674
$y_{R(S)}$, $-y_{R(P)}/B$	0.05	0.16
Propeller		
D_P (m)	0.1206	0.136
P (m)	0.08041	0.09724
Number of blades	5	4
$y_{P(S)}$, $-y_{P(P)}/B$	0	0.16
$\alpha_{(S)}/D_P$	0.63	0.77
Scale ratio	1/55.58	1/16.00

[a] For one rudder

starboard motions [10]. The coefficient $L_{R(S)}$ was earlier estimated from free-running zigzag experiments by a trial and error method [10]. However, the coefficient $L_{R(S)}$ has more influence on turning experiments when the sway and yaw velocities are significant. Therefore, the coefficients $\gamma_{R(S)}$ and $L_{R(S)}$ are further investigated for the SPTR system.

The captive model tests for model ship A were carried out in the towing tank of Osaka University. The details of the towing tank are available in [11, 15]. Furthermore, the free-running experiments were conducted in the manoeuvring pond of Osaka University. A brief description of the free-running experiment system of Osaka University will be provided. In this system, a DC motor propels the ship model. The propeller revolutions are measured and recorded during the experiment and the recorded data is used to keep the propeller revolution constant by the onboard computer through feedback control. The heading angle and yaw rate are measured by an optical gyroscope and recorded in the onboard computer. The ship's position is measured by a RTK GPS unit (Trimble, CA, USA) that has an accuracy of ±0.03 m and recorded in the onboard computer. Each rudder is turned using a 5-phase stepping motor, and the rudder angle is controlled via the onboard computer. The wind speed and direction are measured by an anemometer (Novalynx) fitted onboard the ship. The experiments in the towing tank and manoeuvring pond were conducted corresponding to deep-water conditions.

3.1 Estimation of flow-straightening related coefficients

The inflow velocity to a different rudder system during manoeuvring motion is shown in Fig. 4. Regarding the SPSR system, there is minor asymmetry in the inflow to the rudder due to the rotational motion of the propeller. Similarly, for the TPTR system since each rudder is behind the centreline of a single propeller, there is minor asymmetry in the inflow to the rudder due to the rotational motion of the propeller. For the TPTR system, due to a larger lateral distance between the two rudders, there is less interaction between the rudders. For the SPTR system, the two rudders are in close proximity and behind a single propeller, offset from the propeller's centreline. Therefore, the inflow to the port rudder is greatly influenced by the starboard rudder and vice versa during the ship's manoeuvring motions. Besides, the asymmetry due to the propeller rotation direction is more severe because the rudders are not in the propeller's centreline. For the SPSR system, the coefficient L_R has been estimated as nearly equal to $2x_R$ [1]. For the SPTR system, the variation of the coefficients $\gamma_{R(S)}$ is determined from oblique towing tests [15], while the variation of the coefficients $L_{R(S)}$ is determined from free-running experiments. During oblique towing tests, the inflow angle to the rudder is estimated by determining the angle at which normal rudder force is zero. The ship's yaw rate is fixed ($r = 0$). Accordingly, Eqs. 5, 6, 9 and 13 can be simplified as shown in Eq. 15.

$$\gamma_{R(S)} = -\frac{u_{R(S)}}{\nu}\tan\left(\delta_{(S)} - \delta_{0(S)} - \delta_{(S)(P)}\right) \tag{15}$$

From the different parameters recorded during the experiments, all the terms on the RHS of Eq. 15 can be estimated and $\gamma_{R(S)}$ is determined. It is noted that w_R and w_p may vary during the ship's manoeuvring motions [1]. The variation of $w_{P(S)}$ for the SPTR model proposed by Kang et al. [10] was used for analysis. The variation of $w_{R(S)}$ is considered by assuming $\varepsilon_{(S)} = \frac{1-w_{R(S)}}{1-w_{P(S)}}$. During free-running experiments, the rudder normal force is not zero and coefficients $L_{R(S)}$ have to be determined directly from Eqs. 5, 6, 9, and 13. The parameters recorded during the

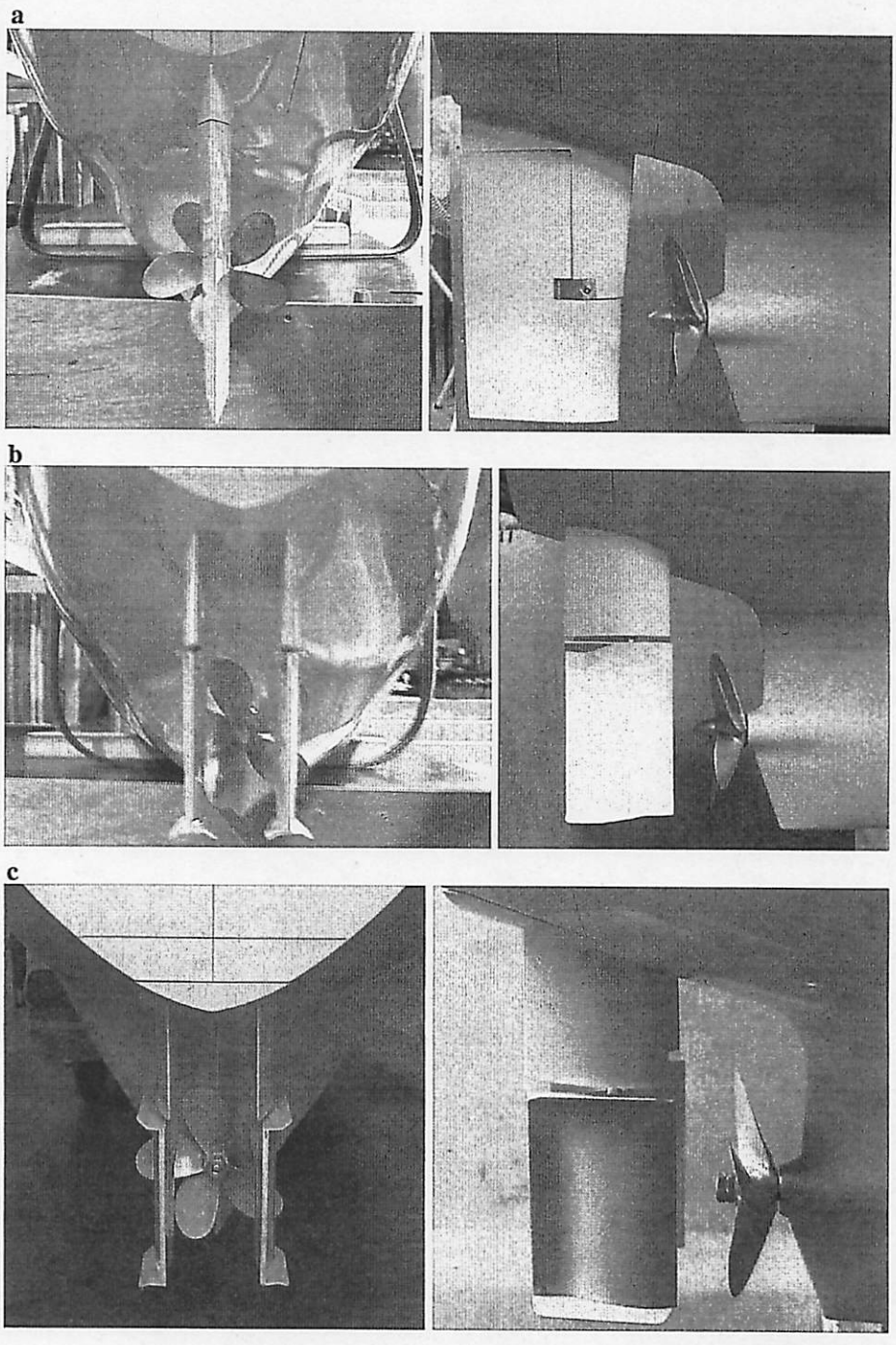

Fig. 2 **a** *Side view* and *stern view* of the single-propeller single-rudder system for model ship A. **b** *Side view* and *stern view* of the single-propeller twin-rudder system (type I) for model ship A. **c** *Side view* and *stern view* of the single-propeller twin-rudder system (type II) for model ship A

Fig. 3 *Side view* and *stern view* of the twin-propeller twin-rudder system for model ship B

Table 2 Comparison of the principal particulars and lateral distance between the rudders and propellers of TPTR model ships

Particulars	Model ship B	TPTR model ship [2, 3]	Wide-beam TPTR model ship [4]	Conventional TPTR model ship [4]
L/B	4.70	3.90	3.70	5.44
B/d	3.02	7.79	5.35	3.60
$y_{P(S)}/B$	0.16	0.20	0.28	0.15

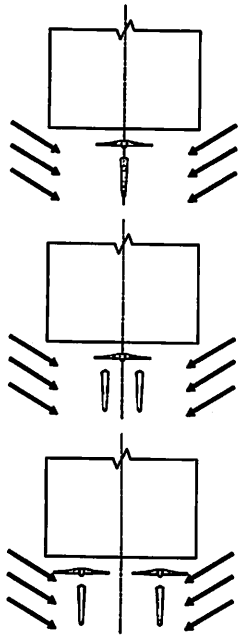

Fig. 4 Inflow to a single-rudder and a twin-rudder system during the ship's manoeuvring motions

Table 3 Parameters considered to determine $L_{R(S)}, \gamma_{R(S)}$ (P) (P)

Parameter	Estimation method
$F_{RY(S)}$ (P), u, v, r, n, $\delta_{R(S)}$ (P)	Recorded by sensors during experiment
$\delta_{(S)}$ (P) $- \delta_{(S)}$ (P) $- \delta_{(S)(S)}$ (P)(P)	Regression using towing tank experiment results (SPTR system)
$\alpha_{R(S)} = \delta_{(S)} - \delta_{R(S)}(\beta_{R(S)})$ (P) (P) (P) (P)	Eqs. 7, 8 (TPTR system)
$u_{R(S)}, v_{R(S)}$ (P) (P)	Eqs. 11, 12 and 13
$w_{R(S)}$ (P)	Kang et al. [10] for SPTR system MMG definition [1] applied to TPTR system
$w_{P(S)}$ (P)	Kang et al. [10] for SPTR Regression using CMT experiments for TPTR system
ρ, $S_{R(S)}$ (P), $x_{R(S)}$ (P), $x_{P(S)}$ (P), $y_{R(S)}$ (P), $y_{P(S)}$ (P)	Known constants
$F'_{RY(S)}$ (P) $(\alpha_{R(S)})$ (P)	Rudder open-water tests

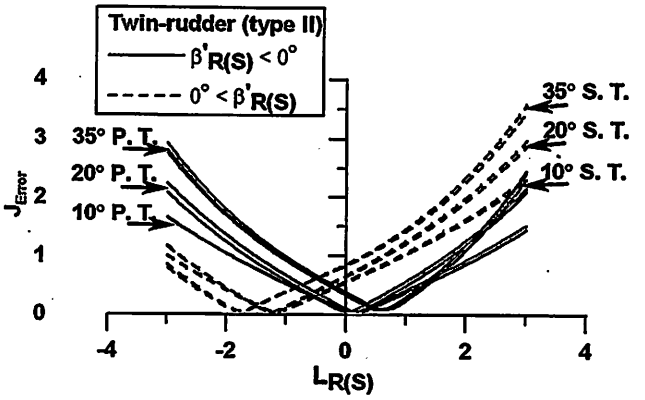

Fig. 5 Error function variation while estimating flow-straightening coefficient for model ship A (*P. T.* port turning, *S. T.* starboard turning)

experiments are shown in Table 3. For the SPSR system, we determine γ_R from the free-running experiment since L_R is estimated to be ($=2x_R$) [1]. For the SPTR system, we determine $L_{R(S)}$ (P) from the free-running experiment since $\gamma_{R(S)}$ (P) is known from the captive test. The hill-climbing procedure is used, $\gamma_{R(S)}$ (P) or $L_{R(S)}$ (P) for which J_{Error} is the minimum is selected as shown in Eq. 16.

$$J_{Error} = \frac{1}{T}\sum_{t=0}^{t=T}\left|F_{RY(S)} - \frac{1}{2}\rho S_{R(S)} F'_{RY_{(S)}}\left(\alpha_{R(S)}\right) U^2_{R(S)}\right| dt \tag{16}$$

The variation of error function for model ship A fitted with the SPTR system is shown in Fig. 5. Each line shows the variation of the error function for different values of flow-straightening coefficient for a particular free-running experiment. In order to check the repeatability of the phenomena, the same experiments were repeated twice. This can be seen as two lines in the figure. Solid lines are cases where the effective drift angle at rudder position is negative (port turning) while the dotted lines are cases where the effective drift angle at rudder position is positive (starboard turning). For an experiment, the optimum flow-straightening coefficient is the one where the error function is the minimum. The optimum flow-straightening coefficient for the SPSR system estimated from free-running experiments, following the above mentioned procedure, is shown in Fig. 6. The flow-straightening coefficient is positive for ship's port and starboard motions. Additionally, there is a small asymmetry in the numerical values of the flow-straightening coefficient for ship's port and starboard motions. This could be due to the

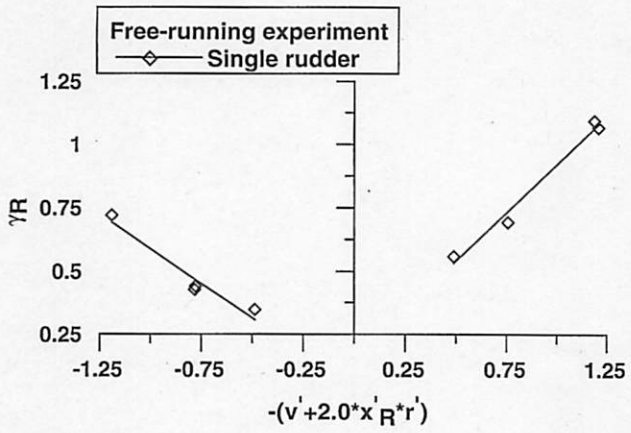

Fig. 6 Variation of γ_R for single-propeller single-rudder system, $L_R = 2x_R$ for model ship A

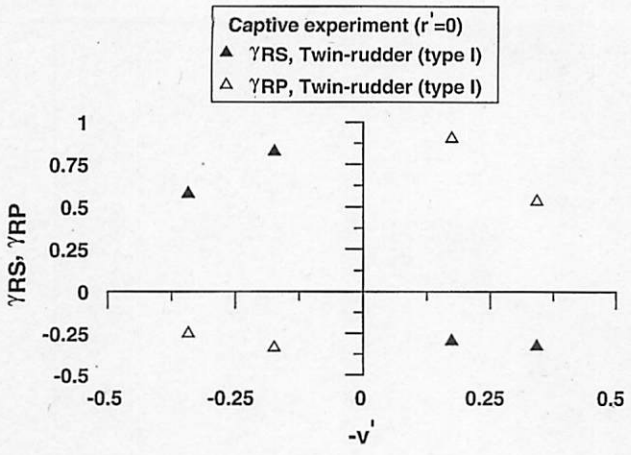

Fig. 7 Variation of $\gamma_{R(S)}$ for single-propeller twin-rudder system of model ship A

propeller rotation direction. For the SPTR system, the flow-straightening coefficient determined from the oblique towing tests ($r = 0$) is shown in Fig. 7. The asymmetry is severe regarding the SPTR system. This may be due to the combined effects of the propeller rotation direction and the close proximity of the rudders behind a single propeller.

The coefficient $L_{R(S)}$ estimated from the free-running experiment and using $\gamma_{R(S)}$ values from oblique towing tests (Fig. 7) for the SPTR system is shown in Fig. 8. Because of the proximity of the rudders, the space is insufficient to fit two load cells at the same time. Therefore, each experiment was carried out twice (once with a load cell on the starboard rudder and once with a load cell on the port rudder). The coefficient $L_{R(S)}$ is observed to be asymmetric for the ship's starboard and port manoeuvring motions. Additionally, the coefficient $L_{R(S)}$ is influenced by the type of twin-rudder (type I and type II

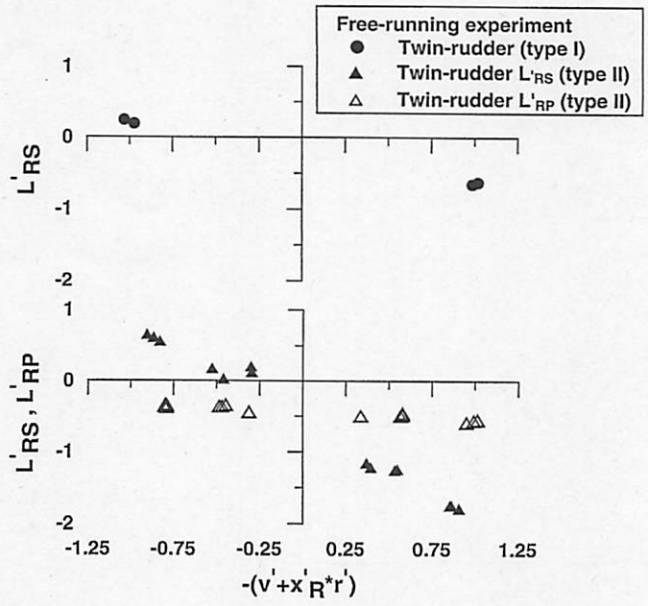

Fig. 8 Variation of $L_{R(S)}$ for different types of single-propeller twin-rudder systems of model ship A (single-propeller twin-rudder ship). $\gamma_{R(S)}$ values are from the oblique towing test

twin-rudders have different cross-sections). The coefficient $L_{R(P)}$ shows a different trend from $L_{R(S)}$ variation as it is shown in Fig. 8. This asymmetry may be due to the following two reasons: the twin-rudders are located behind a single propeller. The propeller rotates clockwise when seen from behind the ship for ahead-motion. Therefore, the flow stream on the port and starboard rudders is not the same for port and starboard turns. The other reason is that during a port turn the starboard rudder (outboard rudder) seems to block the flow to the port rudder (inboard rudder) and vice versa.

3.2 Validation of the asymmetric behaviour of twin-rudder normal force

Using the mathematical model developed earlier, simulations in the time domain were carried out to examine its validity. The simulation of a turning experiment with the SPSR system is shown in Fig. 9. The rudder normal force and yaw rate predicted by simulation are marginally different from the experiment values. The difference in trajectory predicted by simulation and experiment is relatively higher. There are two reasons for this phenomenon. The first reason is that during the subject model ship free-running experiments, the sources of error from different sensors were investigated [16]. It is shown that the maximum contribution to the uncertainty of the experiment result is from the error in measuring the heading angle and speed. The model ship's trajectory is measured by integrating $\dot{x}_E$ and $\dot{y}_E$ obtained by Eq. 17 for the duration of the experiment.

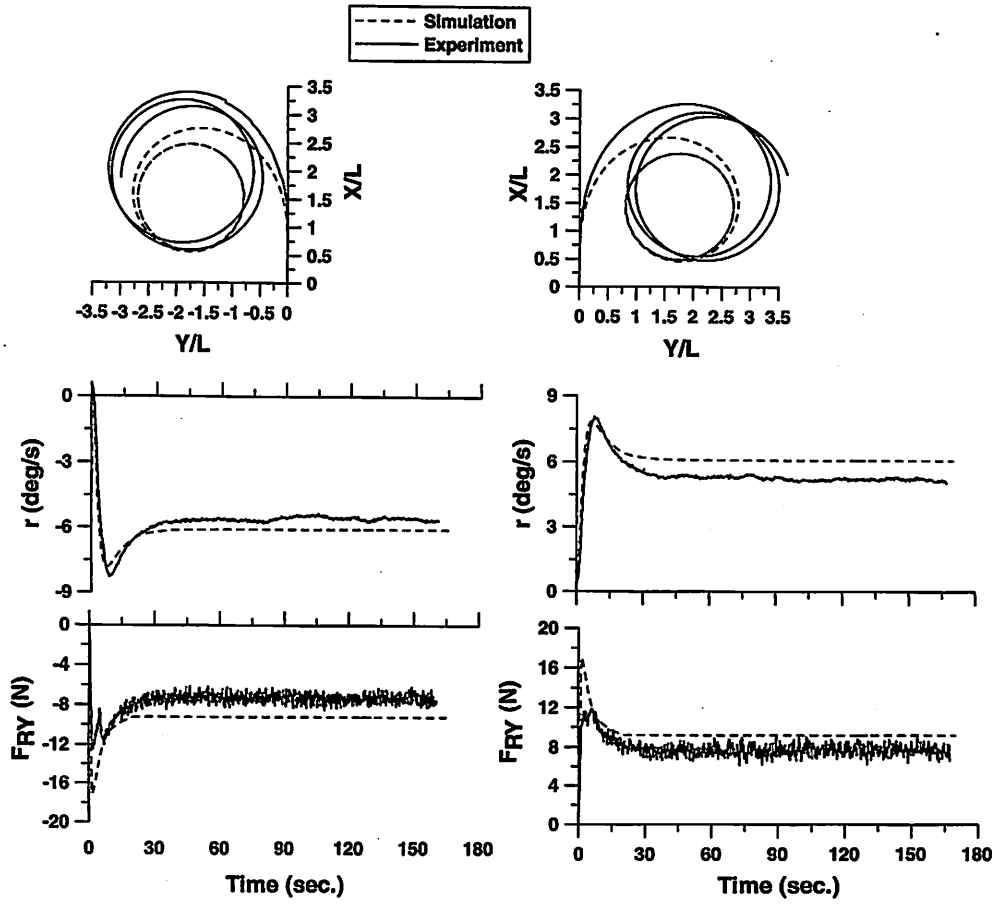

Fig. 9 Comparison between the free-running experiment and simulation results of the single-propeller single-rudder during turning tests ($\delta = \pm 35°$). Initial speed $U = 1.09$ m/s, rps = 17.2 (model ship A)

$$\begin{bmatrix} \dot{x}_E \\ \dot{y}_E \end{bmatrix} = \begin{bmatrix} \cos\psi & -\sin\psi \\ \sin\psi & \cos\psi \end{bmatrix} \begin{bmatrix} u \\ v \end{bmatrix} \tag{17}$$

When estimating the trajectory, the error keeps adding up. Therefore, unlike other parameters, which are instantaneous readings, the trajectory usually shows higher variation from simulation values. The second reason that contributes to the difference between the simulation and experiment will now be described. During simulation, the hydrodynamic hull forces were estimated by Kijima's regression formula and the hull-rudder interaction coefficients were estimated using MMG models. The stern hull form below the propeller shaft centreline for the subject model ship is different from the conventional hull form for tankers. The yaw-damping effect by the skeg-like stern profile is estimated to be remarkable in the area below shaft centre where wake is small. However, the model could reasonably simulate rudder normal force and the model ship's yaw rate for a different set of experiments.

The rudder normal force is symmetric for ship's port and starboard turns. The simulations of turning experiments $\left(\delta_{\substack{(S)\\(P)}} = \begin{Bmatrix} \pm 10° \\ \pm 10° \end{Bmatrix}\right)$ with a twin-rudder (type II) system are shown in Fig. 10. During free-running experiments, starboard and port rudder normal forces were measured and recorded by repeating the same experiment twice for the reasons described in Sect. 3.1. The simulated rudder normal force agrees well with the experiment results. The rudder normal force for port and starboard turns is asymmetric and its values for port and starboard turns are different. Interestingly, during a starboard turn $\left(\delta_{\substack{(S)\\(P)}} = \begin{Bmatrix} +10° \\ +10° \end{Bmatrix}\right)$, with positive rudder angle, the normal force of port and starboard rudders is negative. This shows that the model ship is turning to the starboard direction even though the rudder normal force is negative.

The simulations of turning experiments $\left(\delta_{\substack{(S)(P)\\(P)(S)}} = \begin{Bmatrix} -30° \\ -40° \end{Bmatrix}, \delta_{\substack{(S)(P)\\(P)(S)}} = \begin{Bmatrix} 40° \\ 30° \end{Bmatrix}\right)$ with a twin-rudder (type II) system are shown in Fig. 11. Regarding this case, the asymmetry of rudder normal force for port and starboard turns is also significant. For a port turn, the rudder normal force is about −9.0 N; however, for starboard turns, the rudder normal force is about 2.0 N. Surprisingly, the turning performance seems to be the same in both cases. The simulated rudder normal force has some minor deviation from the experiment results. However, the asymmetry of rudder normal force for port and starboard

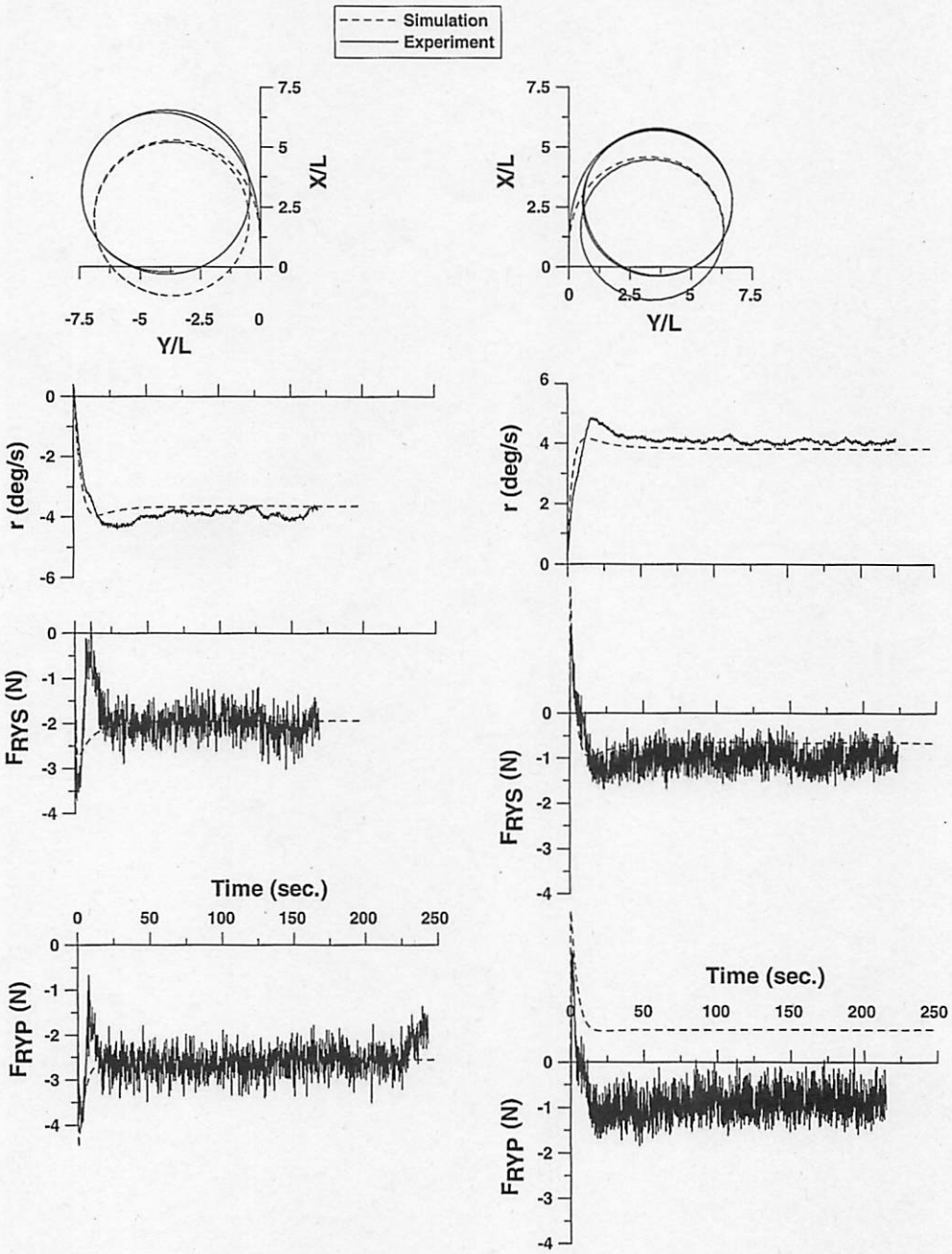

Fig. 10 Comparison between the free-running experiment and simulation results of the single-propeller twin-rudder system (type II). *LHS* ($\delta_{(S)}_{(P)} = \{^{-10°}_{-10°}\}$), *RHS* ($\delta_{(S)}_{(P)} = \{^{+10°}_{+10°}\}$). Initial speed $U = 1.05$ m/s, rps = 17.7 (model ship A). The trajectory shown is for an experiment with load cell on the starboard rudder

turns could be simulated. The hull coefficients including some extra nonlinear terms need to be further investigated to predict the rudder normal force and the turning moment on the hull regarding the SPTR system.

4 Determination of hull-rudder interaction coefficients for twin-propeller twin-rudder system

For the TPTR system, CMT (Circular Motion Tests) tests have been used to determine all the coefficients of the MMG model [2–4]. For the model ship B (TPTR system), CMT experiments were carried out to determine all the parameters of the MMG model, and free-running tests were carried out to validate the MMG model. Here, the authors will validate the method of estimating $\gamma_{R(S)}_{(P)}$ from the free-running experiments. The validation has been done by comparing the values of $\gamma_{R(S)}_{(P)}$ determined from free-running and CMT experiments. Additionally, authors will also discuss the peculiar behaviour of rudder normal force, which was observed for the TPTR system. Similar peculiar behaviour, but of a different pattern, has been showed for the SPTR system in Sect. 3.2. The free-running and CMT experiments were conducted at the sea-keeping and

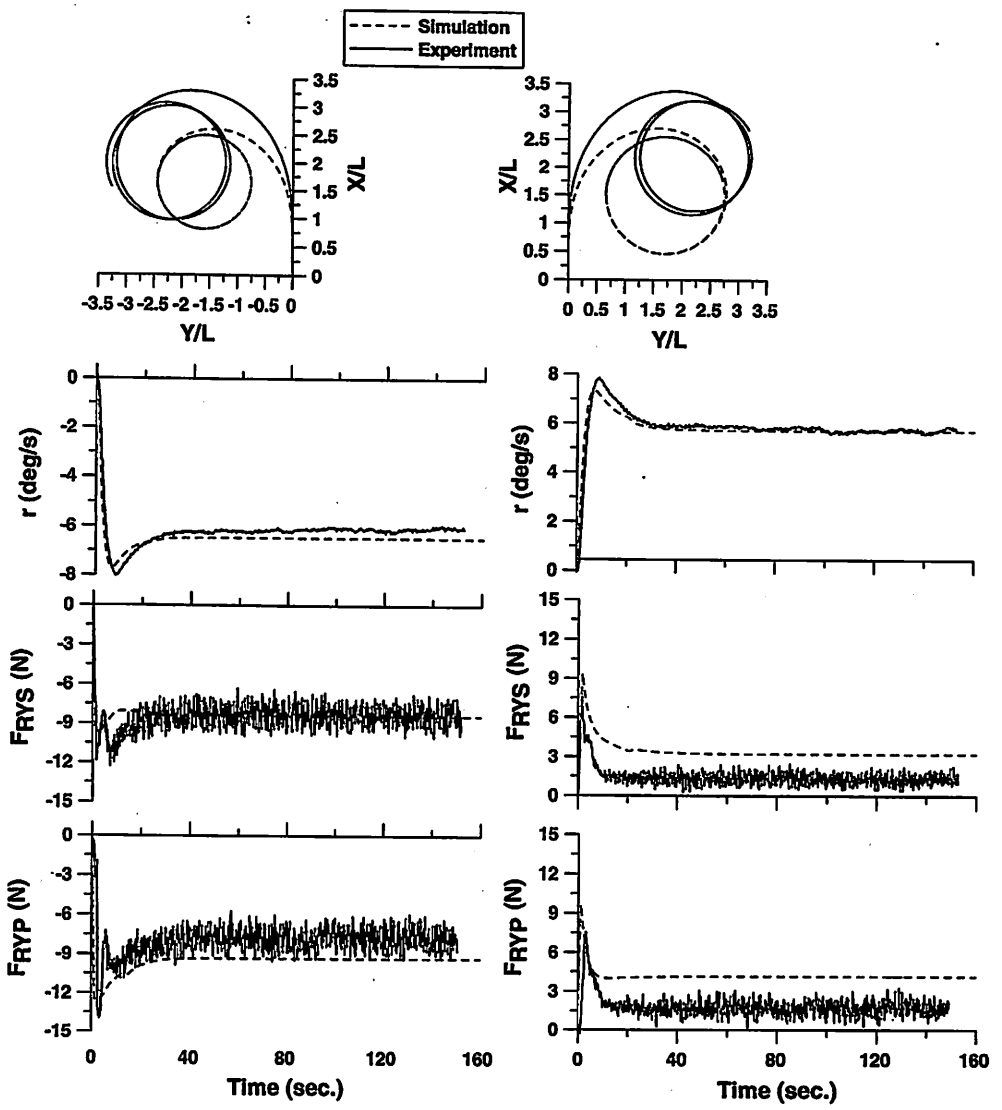

Fig. 11 Comparison between the free-running experiment and simulation results of the single-propeller twin-rudder system (type II). *LHS* ($\delta_{(S)}_{(P)} = \{^{-30°}_{-40°}\}$), *RHS* ($\delta_{(S)}_{(P)} = \{^{40°}_{30°}\}$). Initial speed $U = 1.05$ m/s, rps = 17.7 (model ship A). The trajectory shown is for an experiment with load cell on the starboard rudder

manoeuvring tank of IHI Corporation [17]. The experiments were conducted corresponding to deep water conditions. During CMT experiments, the model ship was operated at model self-propulsion point. This corresponds to a speed of 0.643 m/s with a propeller revolution of 7.97 rps. The drift angle β was varied from 0° to ±25°, and the dimensionless yaw rate was changed from 0 to ±0.7. During both the CMT and free-running experiments, propeller revolution is kept constant by the model ship's computer control system.

4.1 Estimation of flow-straightening related coefficients

Nikolaev [18] carried out rotating arm tests for tanker models in order to study the interaction forces. He concluded that for TPTR models, the interaction force increases with the distance between the propeller shafts where the two rudders are fixed behind the propellers. The interaction reduces again with a further increase of the same distance. Additionally, for TPTR ships, $L_{R(S)}_{(P)}$ is estimated to be between $x_{R(S)}_{(P)}$ [2, 3] to 2.06 $x_{R(S)}_{(P)}$ [4]. It is noted that w_R and w_p may vary during the ship's manoeuvring motions [1]. The variation of $w_{P(S)}$ for the subject TPTR system was determined from the CMT experiment, and it is shown in Fig. 12. It is reported that the coefficient $w_{P(S)}$ will either decrease asymmetrically [2, 3] or remain steady [4] for the TPTR system during manoeuvring motions. For the subject TPTR system, the coefficient $w_{P(S)}$ is found to either remain steady or increase linearly. Moreover, the behaviour is asymmetric for port and starboard motions. The variation of

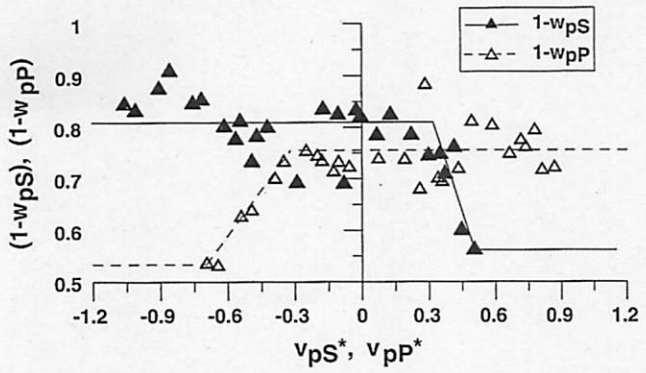

Fig. 12 Variation of the effective wake fraction during turning manoeuvres of starboard and port propeller (model ship B). $v_{P(S)}^{*} = v_{P(S)}' + \tan^{-1}(y_{P(S)}/x_{P(S)})$ and $v_{P(S)}' = -\sin\beta + x_{P(S)}' r'$

$w_{R(S)}$ is considered by assuming $\varepsilon_{(S)} = \frac{1-w_{R(S)}}{1-w_{P(S)}}$ to be constant. The coefficient $\varepsilon_{(S)}$ for the TPTR system is estimated as 0.97 [2, 3] and 0.98 [4]. For the subject TPTR system, the coefficient $\varepsilon_{(S)}$ is assumed as 0.97.

The procedure to determine $\gamma_{R(S)}$, $L_{R(S)}$ from free-running experiments will be described. The parameters recorded during the experiment are shown in Table 3. For the subject model, the coefficients $L_{R(S)}$ and $\gamma_{R(S)}$ were assumed to vary from $0.5 * x_{R(S)}$ to $3.0 * x_{R(S)}$ and -1.0 to 1.75, respectively. Using the hill-climbing procedure, the error function based on Eq. 16 was used to determine the optimum value of each coefficient. The minimum value of the error function, which corresponds to the most optimal values of $L_{R(S)}$ and $\gamma_{R(S)}$, is plotted in the three-dimensional graph of Fig. 13. It is represented by the spherical shapes. The projections of the 3D variation on the (x, z) and (x, y) planes are respectively represented by square and diamond shapes. The minimum error function value does not significantly change for different increments of $L_{R(S)}$. The most suitable value that corresponds to the free-running experiment results corresponds to the one where $L_{R(S)} = x_{R(S)}$. However, there is a wide range of $\gamma_{R(S)}$ for different values of $L_{R(S)}$ where the error function is the minimum. Therefore, further optimization is carried out to determine $\gamma_{R(S)}$, while considering $L_{R(S)} = x_{R(S)}$.

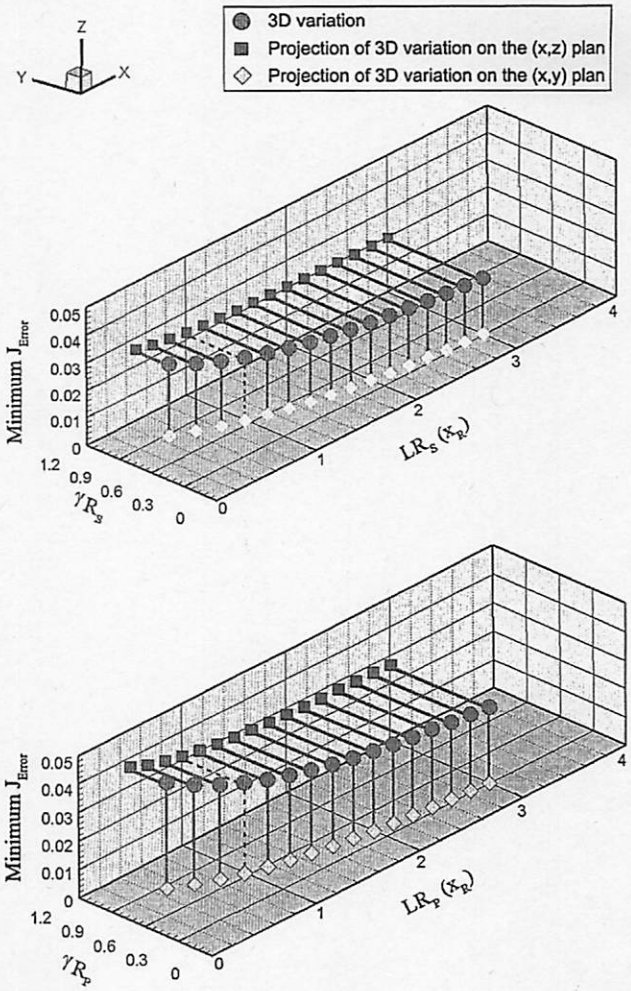

Fig. 13 Variation of $L_{R(S)}$, $\gamma_{R(S)}$ and error function J_{Error} from free-running experiments (model ship B, twin-propeller twin-rudder ship). *Dotted lines* refer to the optimum values of $\gamma_{R(S)}$ and $L_{R(S)}$

Using the hill-climbing procedure, the value of $\gamma_{R(S)}$, for which J_{Error} is the minimum, is selected as shown in Eq. 16. Similar to the SPTR system, the error function variation J_{Error} is observed to have a parabolic trend with a single minimum value for each experiment case. The variation is shown in Fig. 14. Each line corresponds to the error function variation while estimating flow-straightening coefficient $\gamma_{R(S)}$ during the free-running experiments. In order to check the repeatability of the phenomena, the same experiments were repeated twice. This can be seen as two lines in the figure. Solid lines show the variation for cases where the effective drift angle at rudder position $\beta_{R(S)}$ is positive (starboard turning). Dotted lines show the variation for the cases where the effective drift angle at rudder position $\beta_{R(S)}$ is negative (port turning). The

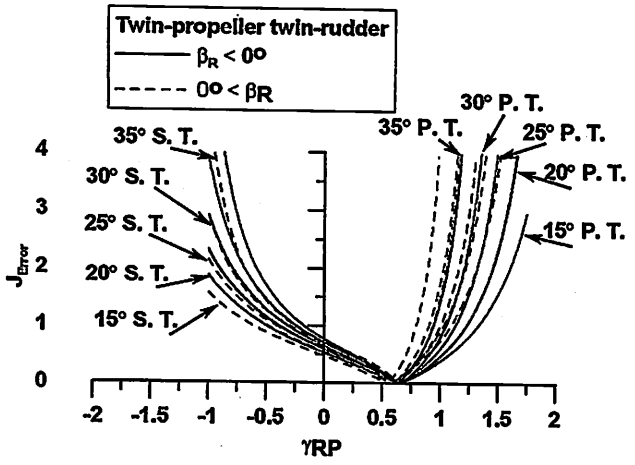

Fig. 14 Error function variation while estimating flow-straightening coefficient for model ship B (twin-propeller twin-rudder ship). A similar trend is observed for error function variation while estimating $\gamma_{R(S)}$. (*P. T.* port turning, *S. T.* starboard turning)

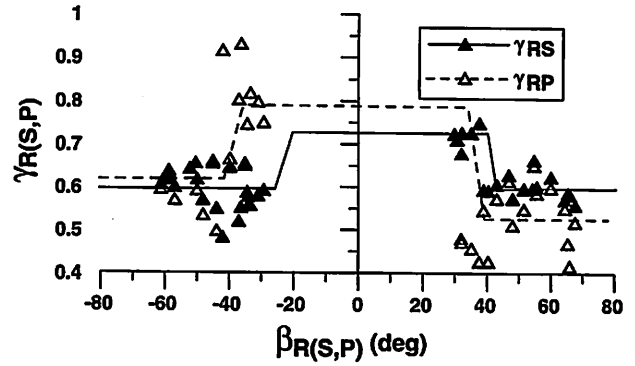

Fig. 15 Variation of $\gamma_{R(S)}$, $L_{R(S)} = x_{R(S)}$ (model ship B, twin-propeller twin-rudder ship)

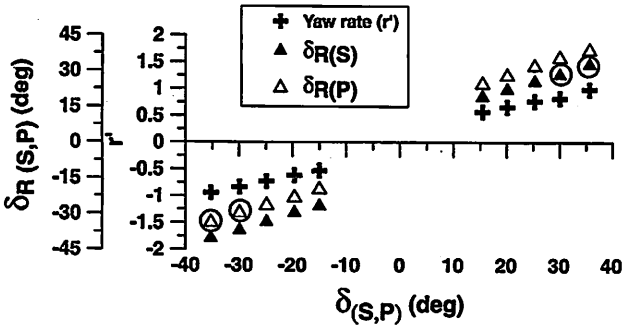

Fig. 16 Average of the steady values of yaw rate and effective rudder angle at which the rudder normal force becomes zero for starboard and port rudder (model ship B, twin-propeller twin-rudder ship)

variation of the coefficient $\gamma_{R(S)}$ is shown in Fig. 15. The flow-straightening coefficient for the TPTR system is asymmetric and different from that of the SPSR and SPTR systems. The coefficient $\gamma_{R(S)}$ is asymmetric for the port and starboard rudders and depends on ship's port and starboard manoeuvring motions. Based on the analyzed values of $\gamma_{R(S)}$, the effective rudder angle $\delta_{R(S)}$ is calculated and the results are shown in Fig. 16. The angle $|\delta_{R(S)}|$, for most of the cases is higher than the angle $|\delta_{(S)}|$. Therefore, from Eq. 6, the effective rudder angle $(\alpha_{R(S)})$ will have an opposite sign to the rudder angle $\delta_{(S)}$. This will result in rudder normal force being exerted in the opposite direction to the rudder angle. We refer to this phenomenon as non-conventional behaviour of the rudder normal force. The conventional cases are the port rudder at $\delta_{(S)} = \{^{+35°}_{+35°}\}$ and $\delta_{(S)} = \{^{+30°}_{+30°}\}$ starboard turning, and for the starboard rudder at $\delta_{(S)} = \{^{-35°}_{-35°}\}$ and $\delta_{(S)} = \{^{-30°}_{-30°}\}$ port turning. For easy understanding, these cases are bordered with circles in Fig. 16. The reason for the asymmetric behaviour of $\gamma_{R(S)}$ and non-conventional sign of rudder normal force will be discussed in Sect. 4.3 with free-running experiment results.

4.2 Validity of estimation method

The coefficient $\gamma_{R(S)}$ determined from free-running and CMT experiments will be compared. During CMT experiments, the rudder normal forces for both rudders were measured. The experiment data was used to determine the neutral rudder angle during manoeuvring. Neutral rudder angle is the angle at which the rudder normal force becomes zero, even though the ship is turning, and the rudder is deflected. The variation of effective rudder angle $(\delta_{R(S)})$ with respect to the drift angle at rudder position $(\beta_{R(S)})$ is plotted for the data recorded in the free-running test and in CMT experiments. The slope of this curve is the flow-straightening coefficient $\gamma_{R(S)}$. The results are shown in Fig. 17. The flow-straightening coefficient $\gamma_{R(S)}$ from CMT experiments and free-running experiments is asymmetric for port and starboard manoeuvring motions. The values of $\gamma_{R(S)}$ between CMT and free-running experiments are noticeably different. This is because during CMT experiments, model ship speed is kept constant $(\sqrt{u^2+v^2} = \sqrt{u_0^2+v_0^2})$; whereas for the free-running

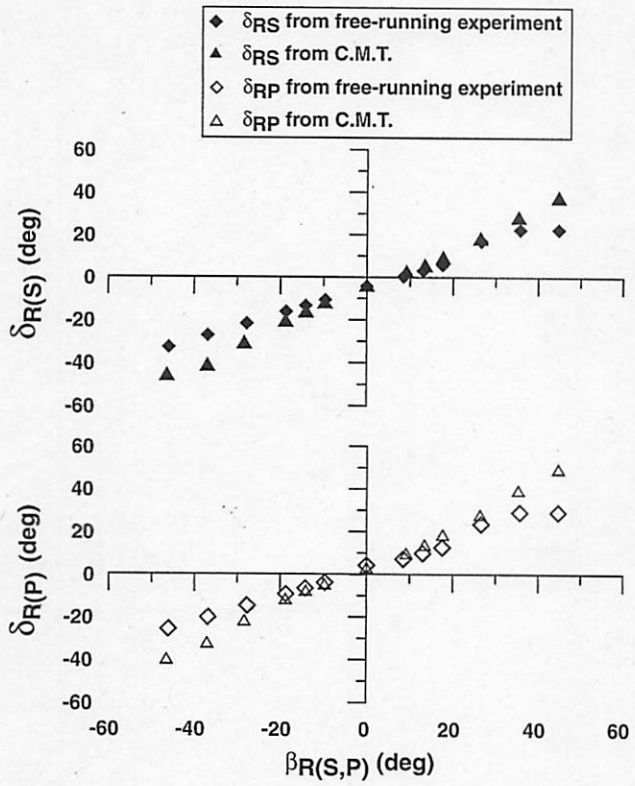

Fig. 17 Variation of $\gamma_{R(S)}$ from the free-running and CMT experiments (model ship B, twin-propeller twin-rudder ship)

experiments, under steady condition of turning motion, the ship's speed decreases from its initial value ($\sqrt{u^2+v^2} < \sqrt{u_0^2+v_0^2}$). It may be noted that the propeller revolution remains constant during both CMT and free-running experiments, and the subject TPTR model ship shows either steady or increasing wake during manoeuvring motion (Fig. 12). Therefore, during free-running experiments, there is an increase in propeller loading due to the extra speed drop during free-running experiments when compared to the CMT experiments. For this reason, the non-dimensional yaw rate (r'), the drift angle at rudder position ($\beta_{R(S)}$), and the rudder angle at which rudder normal force is zero during ship's manoeuvring ($\delta_{R(S)}$) for CMT and free-running experiments are different. This shows that the flow-straightening coefficient at model and ship propulsion points may be different. Besides it may also be influenced by the rps decrease during full-scale manoeuvring.

4.3 Simulation of free-running experiments

The validation of the MMG model developed for the subject TPTR system will be conducted using free-running experiments. The peculiar behaviour of rudder normal force observed during free-running experiments and the need to incorporate them in the proposed model will be discussed. Free-running, turning, and zigzag tests were carried out in order to examine different hydrodynamic aspects of the subject ship B. Free-running experiments were conducted at two different speeds U (initial speed) = 0.643 m/s, rps = 7.97 and U (initial speed) = 1.029 m/s, rps = 12.8, which correspond to the actual ship operating (5 knots) and cruising speed (8 knots) conditions. The hull and rudder interaction coefficients have been described in the paper. The remaining coefficients of the mathematical model are given in the Appendix I. The experiment and simulation results of turning test for the rudder angles ($\delta_{(S)} = \{^{\pm 15^\circ}_{\pm 15^\circ}\}$) at the ship's initial speed $U = 0.643$ m/s is shown in Fig. 18. In this case, the outboard rudder (starboard rudder in port turning and port rudder in starboard turning) also have the opposite rudder normal force sign to the yaw rate and, therefore, to the turning direction. The proposed model can simulate the trend of the rudder normal force and the ship's yaw rate observed during experiments. During the turning motion, the normal force for inboard rudder also has the opposite sign to the yaw rate and to the turning direction. It shows a lot more difference between experiment and simulation. The difference in trajectory predicted by model free-running experiment and simulation is relatively lower when compared to Fig. 9. In this case, the model ship's position is measured by a supersonic wave-detection sensor. The experiment measurements are not influenced by environmental conditions that affect the RTK-GPS system used for the SPTR system (Fig. 9). The free-running experiments and simulation results of turning test for the rudder angles ($\delta_{(S)} = \{^{\pm 35^\circ}_{\pm 35^\circ}\}$) at the ship's initial speed $U = 0.643$ m/s are shown in Fig. 19. In this case, the inboard rudder (starboard rudder in starboard turning and port rudder in port turning) has the same rudder normal force sign to the yaw rate, and consequently to the turning direction. However, the outboard rudder has the opposite rudder normal force sign to the turning direction. The simulation can accurately capture the trend of the outboard rudder normal force and the ship's yaw rate, and the difference between simulation and experiment for inboard rudder normal force is higher. The rudder normal force for port and starboard turns is asymmetric, and the pattern of asymmetry is different from that of the SPTR system. The proposed model was used to simulate the rudder normal force for the zigzag experiments. The experiments and simulation results are shown in Fig. 20. In this case, the direction of rudder normal force is opposite to the turning motion. The rudder normal force during a zigzag manoeuvre can be simulated very well. It can be concluded that when there is less nonlinearity, the proposed model works well.

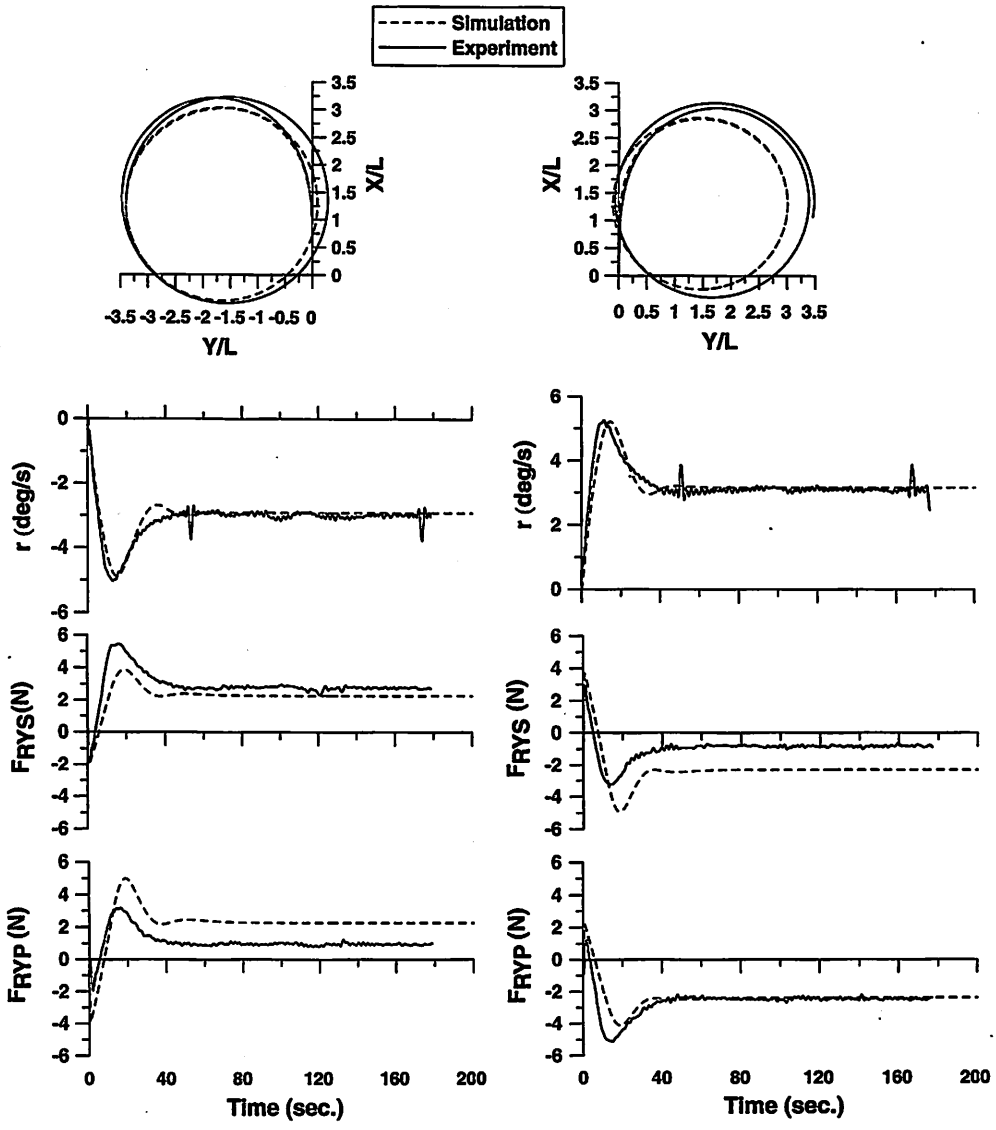

Fig. 18 Comparison between the free-running experiment and simulation results of the twin-propeller twin-rudder system. *LHS* ($\delta_{(S)}_{(P)} = \{^{-15°}_{-15°}\}$), *RHS* ($\delta_{(S)}_{(P)} = \{^{-15°}_{-15°}\}$). Initial speed $U = 0.643$ m/s, rps = 7.97 (model ship B)

However, regarding steady-turning motion, the nonlinear phenomenon is severe, which the present model cannot fully capture. In both the TPTR and SPTR systems, the rudder is offset from the ship's centreline. In the TPTR system, the rudder is at the propeller's centreline. In the SPTR system, the rudder is offset from the propeller's centreline. This may influence $\gamma_{R(S)}_{(P)}$ and $L_{R(S)}_{(P)}$ coefficients for the SPTR system when compared to the TPTR system. For the subject TPTR model ship, the lateral distance between the rudders is higher than that of the SPTR system (Table 1). This lateral distance is comparable to other conventional TPTR systems (Table 2). For both model ship A (SPTR) and B (TPTR), the values of $\alpha_{(S)}_{(P)}$ are relatively higher than those for conventional ships, as mentioned in Sect. 2.2. This may be contributing to the change in the direction of inflow to the rudder during manoeuvring motions, resulting in the non-conventional sign of rudder normal force phenomenon for the SPTR and the subject TPTR systems. Further work in this direction is necessary to draw firm conclusions.

5 Conclusions

In this paper, manoeuvring characteristics at the cruising speed of a ship fitted with twin-rudder systems has been investigated. The conclusions of this paper are as follows:

1. For twin-rudder systems, the effective inflow angle could go in the opposite direction to the rudder angle during turning motions. For a single-propeller twin-rudder system, this phenomenon is usually observed for a lower range of rudder angle. For a twin-propeller twin-rudder system, the phenomenon seems to be more significant and could be observed for the entire operating range of the rudder angle.

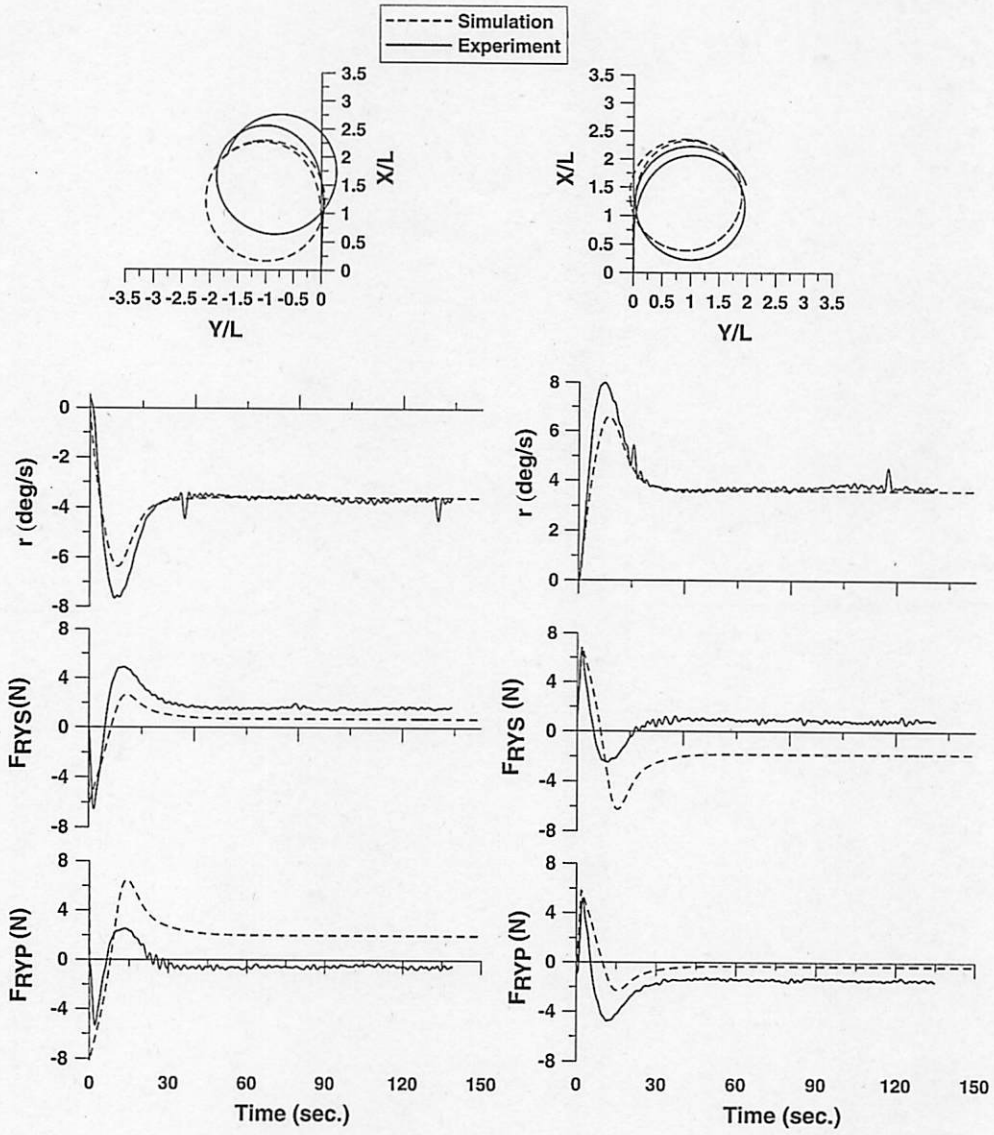

Fig. 19 Comparison between free-running experiment and simulation results of the twin-propeller twin-rudder system. *LHS* ($\delta_{(S)}_{(P)} = \{^{-35°}_{-35°}\}$), RHS: ($\delta_{(S)}_{(P)} = \{^{-35°}_{-35°}\}$). Initial speed $U = 0.643$ m/s, rps = 7.97 (model ship B)

2. A method for estimating rudder hull-interaction coefficients for different rudder systems is proposed. The proposed method is based on the hill-climbing procedure. An error function is defined, and it is shown that minimum value of the error function corresponds to the optimal value of the coefficients $\gamma_{R(S)}$ and $L_{R(S)}$.
3. The flow-straightening coefficient shows a slight asymmetric behaviour for starboard and port turning for a single-propeller single-rudder system. This coefficient is significantly asymmetric in the case of a single-propeller twin-rudder system, but shows a slight asymmetric trend for a twin-propeller twin rudder system.
4. For the TPTR system, $L_{R(S)}$ is estimated to be nearly as follows $L_{R(S)} = x_{R(S)}$. Regarding the SPTR system, $L_{R(S)}$ is considered to be variable and its variation is asymmetric not only for starboard and port rudders but also for starboard and port turns.
5. Further investigations and experiments are required for model ships A and B in order to investigate the nonlinear effect and different interactions between rudders and propellers during steady turning. The modified mathematical model for simulating the opposite sign of rudder normal force during manoeuvres needs to be improved, and further work in this direction is being carried out.

Acknowledgments The experiments on the single-propeller twin-rudder system were supported by Japan Hamworthy Co. Ltd. The authors are grateful for their collaboration and contribution. The authors also thank Mr. Y. Gonno and Mr. Y. Uematsu, Master's course students, Department of Ocean Engineering and Naval

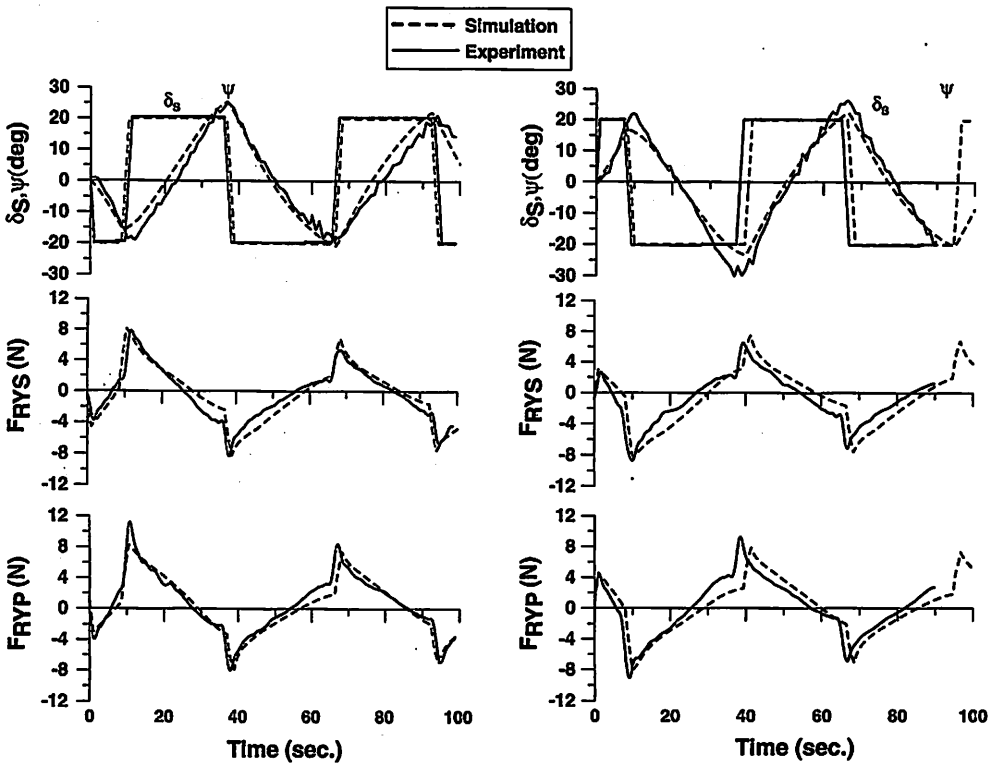

Fig. 20 Comparison between zigzag free-running experiment and simulation results of the twin-propeller twin-rudder system. *LHS* ($\delta_{(S)}^{(P)} = \{^{-20°/-20°}_{-20°/-20°}\}$), RHS: ($\delta_{(S)}^{(P)} = \{^{-20°/-20°}_{-20°/-20°}\}$). Initial speed $U = 0.643$ m/s, rps = 7.97 (model ship B)

Architecture, Osaka University, for their help during experiments with the single-propeller twin-rudder system. The experiments on twin-propeller twin-rudder system were supported by IHI Corporation, Yokohama, Japan. The authors are grateful for their collaboration and contribution. The authors would also like to thank Mr. K. Saitou and Mr. Y. Fukui of IHI Corporation for their help during experiments with the twin-propeller twin-rudder ship.

Appendix I

The coefficients of the TPTR model are given in Table 4. The coefficients of the SPTR model were described in Kang et al. [10], (2008).

Table 4 The coefficients of the TPTR model (model ship B)

Coefficient	Value
m'	0.3404
m'_x, m'_y	0.0387, 0.2467
$I'_{zz} + J'_{zz}$	0.0372
X'_0, $X'_{\|v\|}$, $X'_{\|r\|}$, X'_{vv}, X'_{vr}, X'_{rr}	−0.0217, −0.0130, −0.0080, 0.0708, 0.8720, 0.0172
Y'_v, Y'_r, Y'_{vvv}, Y'_{vvr}, Y'_{vrr}, Y'_{rrr}	−1.3122, 0.3043, 0.0734, −4.9906, −1.1945, −0.0188
N'_v, N'_r, N'_{vvv}, N'_{vvr}, N'_{vrr}, N'_{rrr}	−0.0260, −0.0458, −0.0652, −0.0627, −0.0585, 0.0087
$w_{P0(S)}^{(P)}$	0.1986
$t_{P0(S)}^{(P)}$	0.1009
$w_{R(S)}^{(P)}$	0.2578
a_H	0.7122
$x'_{H_{(S)}^{(P)}}$	−0.3719
$\varepsilon_{(S)}^{(P)}$	0.97

Table 4 continued

Coefficient	Value
$\kappa_{\substack{(S)\\(P)}}$	0.7522
$F'_{RY_{\substack{(S)\\(P)}}}(\alpha_{R_{\substack{(S)\\(P)}}})$	$2.3318 \sin\left(\alpha_{R_{\substack{(S)\\(P)}}}\right)$
$K_{T_{\substack{(S)\\(P)}}}$	$0.3319 - 0.3352\, J_{P_{\substack{(S)\\(P)}}} - 0.1434\, J^2_{P_{\substack{(S)\\(P)}}}$

References

1. Mathematical Modelling Group Report I, II, III, IV and V (1977, 1980) Bull Soc Nav Archit Jpn, 575:192–198, 577:322–329, 578:358–372, 579:404–413 and 616:572–573 (in Japanese)
2. Lee SK, Fujino M, Fukasawa T (1988) A study on the manoeuvring mathematical model for a twin-propeller twin-rudder ship. J Soc Nav Archit Jpn 163:109–118 (in Japanese)
3. Lee SK, Fujino M (2003) Assessment of mathematical model for the manoeuvring motion of a twin-propeller twin-rudder ship. ISP 50:109–123
4. Yoshimura Y, Sakurai H (1989) Mathematical model for the manoeuvring motion in shallow water (3rd report). J Kansai Soc Nav Archit Jpn 211:115–126 (in Japanese)
5. Nakatake K, Ando J, Kataoka K et al (1989) Study on the propulsive performance of twin-screw ship: Interaction between propeller and rudder in uniform flow. Trans West-Japan Soc Nav Archit 78:49–57 (in Japanese)
6. Fung S, Slager J, Wilson M (1989) Hydrodynamic performance of a twin-skeg T-AO. In: Proceedings of 14th Ship Technology and Research (STAR) Symposium, IMSDC 88, New Orleans
7. Hamamoto M, Enomoto T (1997) Maneuvering performance of a ship with VecTwin rudder system. J Soc Nav Archit 181:197–204
8. Hasegawa K, Kang DH, Sano M et al (2006) Study on maneuverability of a large vessel installed with a mariner type super Vectwin rudder. J Mar Sci Technol 11:88–99
9. Japan Hamworthy & Co. Ltd. (2003) http://www.japanham.co.jp
10. Kang DH, Nagarajan V, Hasegawa K et al (2008) Mathematical model of single-propeller twin-rudder ship. J Mar Sci Technol 13:207–222
11. Nagarajan V, Kang DH, Hasegawa K et al (2009) A proposal for propulsion performance prediction of a single-propeller twin-rudder ship. J Mar Sci Technol 14:296–309
12. Khanfir S, Nagarajan V, Hasegawa K et al (2009) Estimation of mathematical model and its coefficients of ship manoeuvrability for a twin-propeller twin-rudder ship. In: Proceedings of MARSIM'09, Panama City, pp M159–M166
13. Kijima K, Nakiri Y (2002) On the practical prediction method for ship maneuvering characteristics. Trans West Jpn Soc Nav Archit 105:21–31 (in Japanese)
14. Zosen sekkei binran (Shipbuilding Design Handbook) (1983), 4th edn. The Kansai Society of Naval Architects, Japan, Tokyo, pp 474–475 (in Japanese)
15. Osaka University, Division of Global Architecture,Graduate School of Engineering, Department of Naval Architecture and Ocean Engineering (2006). http://www.naoe.eng.osaka-u.ac.jp/eng/research/facility.html
16. Kang DH, Nagarajan V, Gonno Y et al (2011) Installing single-propeller twin-rudder system with less asymmetric maneuvering motions. Ocean Eng 38:1184–1196
17. IHI Corporation (2010). http://www.ihi.co.jp/index-e.htm
18. Nikolaev E (1989) Results of rotating arm tests carried out in Kyrlov Shipbuilding Research Institute to investigate flow around ship hull model and interaction forces between hull, propeller and rudder. Working paper for the 19th ITTC Manoeuvrability Committee, Leningrad, p 394